Title: In Situ Hydrogels Enhancing Postoperative Functional Recovery by Reducing Iron Overload after Intracerebral Haemorrhage

Authors: Tiantian Luo, Tingwang Guo, Qian Yang, Shilei Hao, Ju Wang, Zhongjun Cheng, Qing Qu, Ye He, Yuhua Gong, Feiyan Gao, Wenfeng Li, Haijian Xia, Bochu Wang

PII: S0378-5173(17)30960-2
DOI: https://doi.org/10.1016/j.ijpharm.2017.10.010
Reference: IJP 17066

To appear in: *International Journal of Pharmaceutics*

Received date: 4-6-2017
Revised date: 1-10-2017
Accepted date: 4-10-2017

Please cite this article as: Luo, Tiantian, Guo, Tingwang, Yang, Qian, Hao, Shilei, Wang, Ju, Cheng, Zhongjun, Qu, Qing, He, Ye, Gong, Yuhua, Gao, Feiyan, Li, Wenfeng, Xia, Haijian, Wang, Bochu, In Situ Hydrogels Enhancing Postoperative Functional Recovery by Reducing Iron Overload after Intracerebral Haemorrhage.International Journal of Pharmaceutics https://doi.org/10.1016/j.ijpharm.2017.10.010

In Situ Hydrogels Enhancing Postoperative Functional Recovery by Reducing Iron Overload after Intracerebral Haemorrhage

Tiantian Luo,[a, b, 1] Tingwang Guo,[a, b, 1] Qian Yang,[a, b, 1] Shilei Hao,[a, b, *] Ju Wang,[a, b] Zhongjun Cheng,[a, b] Qing Qu,[a, b] Ye He,[a, b] Yuhua Gong,[a, b] Feiyan Gao,[a, b] Wenfeng Li,[a, b] Haijian Xia,[c] Bochu Wang[a, b, *]

[a] Key Laboratory of Biorheological Science and Technology, Ministry of Education, College of Bioengineering, Chongqing University, Chongqing 400030, China.

[b] Collaborative Innovation Center for Brain Science, Chongqing University, Chongqing 400030, China.

[c] Department of Neurosurgery, the First Affiliated Hospital of Chongqing Medical University, Chongqing 400016, China.

∗ Corresponding authors. Tel.:+86 23 6512 0021; Fax: +86 23 6512 0021.

E-mail address: shilei_hao@cqu.edu.cn (S. Hao); wangbc2000@126.com (B. Wang).

[1] These authors contributed equally to this work.

Graphical abstract:

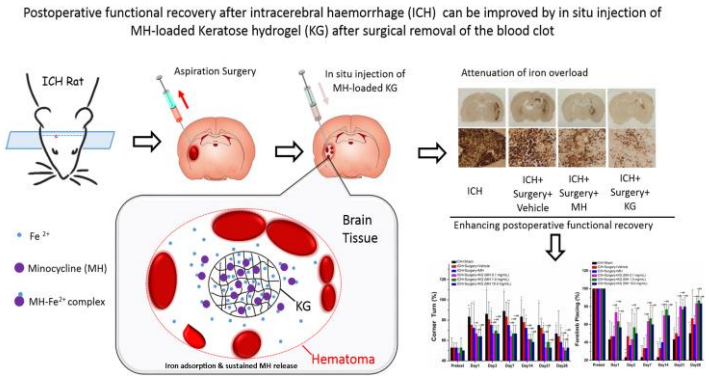

ABSTRACT:

The role of surgery for most patients with spontaneous intracerebral haemorrhage (ICH) remains controversial due to the continuous occurrence of postoperative iron

overload induced by low clot clearance rate. In this study, human hair keratose hydrogel (KG) loading with minocycline hydrochloride (MH) were prepared to reduce iron overload for the improvement of the postoperative functional recovery after ICH aspiration surgery. Hemoglobin-induced iron accumulation in rat primary neuronal culture was delayed by the adsorptive capacity of blank KG, while MH-loaded KG displayed a stronger and more thorough cytoprotective effect than blank KG due to the combined effect of absorptive action to iron and sustained release of the iron chelator. Moreover, high iron-chelating efficiency in the hematoma region supplied by MH-loaded KG significantly reduced dose strength of iron chelator. In situ injection of KG with different MH loadings (2, 20, and 200 μg) into the hematoma region after aspiration surgery showed a stronger effect on the reduction of ICH-induced iron accumulation, edema, and neurological deficits in rats compared to the postoperative intraperitoneal administration of MH (approximately 15 mg). These results suggested that the in situ KG not only could effectively reduce the ICH postoperative iron overload and improve the postoperative functional recovery via the iron adsorption and sustained release of MH, but also has great potential to reduce the systemic adverse effects by decreasing the dose strength of iron chelator.

Keywords:

Intracerebral haemorrhage, Surgery, Iron overload, Human hair keratose, Hydrogels, Minocycline hydrochloride

1. Introduction

Intracerebral haemorrhage (ICH) is an acute and spontaneous extravasation of blood into the brain parenchyma, which is the second most frequently observed subtype of stroke (Mayer and Rincon, 2005; Qureshi et al., 2009). ICH has obtained great attention due to very high mortality and morbidity. The 30-day mortality was approximately 30–55 %, and only 20 % could live independently at 6 months (Balami and Buchan, 2012; Kumar et al., 2016). The risks of spontaneous ICH mainly include hypertension, cerebral amyloid angiopathy, heavy alcohol consumption, anticoagulants

administration, and cigarette smoking (Mayer and Rincon, 2005; Xi et al., 2014). However, the current treatment for ICH is primarily supportive, and the outcomes remain poor (Mayer, 2003).

Surgery treatment for ICH clot removal has potential to prevent herniation and reduce the pathophysiological impact of hematoma on the surrounding tissues (Hemphill et al., 2015; Mendelow et al., 2013). Furthermore, surgery is necessary for patients with a large lobar ICH that produces mass effect and impairs consciousness (Flaherty and Beck, 2013). However, several randomized controlled trials, including the Surgical Trial in Intracerebral Haemorrhage (STICH) trials, have not demonstrated that surgery improved the outcomes beyond medical management (Mendelow et al., 2005; Mendelow et al., 2013). Many factors influence the surgery outcome of ICH, and the quantification of the extent of hematoma evacuation is associated with improved functional outcomes (Ochalski et al., 2014; Rabinstein, 2017). Unfortunately, the average clot clearance rate was about 46 %, and approximately 30 % of patients only reached 80 % clot reduction, which could result in ineffective functional outcomes by the surgery (Morgan et al., 2008; Rabinstein, 2017). In addition, surgery for ICH easily causes the secondary injury induced by blood breakdown and adverse biochemical or inflammatory processes, although it is useful for the reduction of mass effect and improvement of intracranial pressure and brain perfusion. Therefore, the decrease in secondary injury after ICH surgery would contribute to improve postoperative recovery.

Iron generated by hemoglobin degradation is an important metabolic product that accumulates in the brain parenchyma, which can has a detrimental effects following ICH (Xiong et al., 2014). Free iron exhibited 3-fold increase in the cerebrospinal fluids after ICH and remained for at least 28 days (Wu et al., 2003; Xi et al., 2006). Iron overload in the brain causes brain edema in the acute phase of ICH and brain atrophy during the later phases (Xi et al., 2014). Recently, the iron chelators, including deferoxamine and minocycline hydrochloride (MH), have been used to reduce ICH-induced brain edema, neuronal death, brain atrophy, and neurological deficits (Wu et al., 2011; Zhao et al., 2011). One NIH-funded phase I trial has been performed to test the safety and tolerability of deferoxamine in patients with ICH (Selim et al., 2011).

However, many adverse issues, including neurological decompensation, pulmonary embolism and renal failure, were found in the phase I trial, so two subjects (10 %) were prematurely discontinued. Another phase II trial of high-dose deferoxamine in ICH is currently underway (Yeatts et al., 2013). In addition, there were also some concerns about the occurrence of acute respiratory distress syndrome in the phase II trial (Garton et al., 2016).

The aim of this study was to prepare iron chelator-loaded KG to improve the ICH postoperative recovery by reducing iron overload. In situ hydrogel could quickly adsorb the non-heme iron and keep sustained release of the iron chelator, which would contribute to fast reduction of iron overload due to high iron-chelating efficiency. Furthermore, the local delivery strategy has the advantage of reducing the dose strength of iron chelators to decrease the systemic adverse effects.

MH, as an iron chelator, has a clear neurovascular protective effect in the animal models of ICH and ischemic stroke, and the clinical trial of MH in patients with ischemic stroke has been carried out (Garton et al., 2016; Zhao et al., 2011). MH also displayed neuroprotective effect by reducing the inflammatory response to injury. Therefore, MH may show greater protection than an agent targeting iron or inflammation alone (Xi et al., 2014). Meanwhile, keratose was chosen for hydrogel formation due to its well biocompatibility and porous property (Hill et al., 2010; Wang et al., 2017). KGs have shown a great ability for bone regeneration and nerve repair (de Guzman et al., 2013; Pace et al., 2013). The *in vitro* iron adsorption of hydrogel and drug release from hydrogel were investigated in the present study. The cytotoxicity and neuroprotective effects of hydrogel were also evaluated using the primary neuronal cells. Furthermore, the efficacy of MH-loaded KG on functional recovery after ICH surgery in rats was assessed, including iron deposits, brain iron contents, brain edema, and neurological deficits.

2. Materials and methods

2.1 Keratose extraction and hydrogel preparation

Keratose was extracted from human hair using an oxidative method according to

our previous report (Wang et al., 2017). Peracetic acid was selected as an oxidizing agent. The SDS-PAGE and amino acid analysis was performed to evaluate the molecular weight and amino acid composition of keratose, respectively (Wang et al., 2017). KGs were formed by rehydration of the lyophilized keratose with PBS buffer at different concentrations (ranging from 10 % to 40 %, w/v) (de Guzman et al., 2013; Sierpinski et al., 2008). The MH-loaded KGs were prepared by dispersing different MH concentrations (0.1, 1.0 and 10.0 mg/mL) into the keratose solutions.

2.2 Characterizations of KGs

The morphology of KGs with 20 % keratose and 1.0 mg/mL MH was observed by scanning electron microscopy (SEM). The freeze-dried hydrogel was putter-coated using a platinum coater for SEM examination (Tescan VEGA II, LMU, Czech). FT-IR spectra (ranging 400–4000 cm^{-1}) of keratose, MH, and MH-loaded KG (20 % keratose and 1.0 mg/mL MH) were determined by FT-IR spectrophotometer (Nicolet, 5DX/550II, USA). The samples were prepared by grinding the dry specimens with KBr and pressing them to form disks. The XRD analysis was carried out using an X-ray diffractometer (Shimadzu, 6000 X-ray diffractometer, Japan). Keratose, MH, and MH-loaded KG (20 % keratose and 1.0 mg/mL MH) were analyzed in the 2θ ranging from 5 to 45° with a step width of 0.04° and a count time of 2 s.

2.3 Adsorption experiments

Artificial cerebrospinal fluid (CSF) was prepared as the previous report (Andrew and MacVicar, 1994). 100 mg blank KGs with different keratose concentrations (ranging from 10 % to 40 %) were added into 30 mL artificial CSF containing $FeCl_2$ (20 μmol), and the adsorption test was performed at 37 °C in a static water bath. The Fe^{2+} concentration was determined colorimetrically by 1, 10-phenanthroline at 510 nm (Lambda 900, PerkinElmer, USA) (Wang et al., 2009). UV−vis absorption spectra of Fe^{2+} at different time intervals were recorded to monitor the adsorption process. The adsorption capacities of the KGs were calculated according to the equation of $q_e = (C_0 - C_e)$ V/m, where C_0 and C_e was the initial and equilibrium concentrations (μmol),

respectively. *V* is the volume of the solution (mL), and *m* is the amount of the KGs (mg) (Gao et al., 2013).

2.4 Drug release analysis

30 mg MH-loaded KG (20 % keratose and 1.0 mg/mL MH) was added into 5 mL artificial CSF in a tube at 37 °C. At predetermined time intervals, samples were taken and replaced with fresh artificial CSF. Drug concentrations were determined by UV spectrophotometer. Each samplewas performed in triplicate.

2.5 Cell experiments

2.5.1 Cell cultures

Primary neuronal cell culture was performed from pregnant Sprague−Dawley rat embryos on day 18–19 according to the previously described protocols (Borges et al., 2010; Lee et al., 2015).. The use of animals was approved by the Animal Ethics Committee of Third Military Medical University, China. Trypsin was used to dissociate the tissue. Dissociated cells were plated onto 22-mm coverslips coated with 10 μg/mL poly-D-lysine in six-well plates at a density of 150,000 cells/well. The cells were maintained for 21 d in Neurobasal medium containing B27 supplement and 2 mM GlutaMax with half culture medium changed every 7 d.

2.5.2 Cytotoxicity

The cytotoxicity of blank KG (20 % keratose) and MH-loaded KG (20 % keratose and 1.0 mg/mL MH) was evaluated by MTT assay using rat primary neuronal cells. In addition, the *in vitro* cytoprotection of blank KG and MH-loaded KG was also evaluated by MTT assay. Neuronal injury was induced by hemoglobin with different concentrations (ranging from 6.25 to 100 μM). After 4 h, blank KG or MH-loaded KG was added into culture medium and incubated for 24 h.

2.5.3 Immunofluorescence

Cultured cells were fixed in ice-cold 4 % paraformaldehyde in PBS buffer for 20

min and washed 3 times using PBS buffer at predetermined time points. Then the cells were incubated in 1 % BSA in PBS containing MAP2 (Santa Cruz, CA, USA) primary antibody (1:50) for 12 h at 4 °C, followed incubating with Alexa Fluor 488-Labeled Goat Anti-Rabbit IgG (Beyotime Biotechnology, Shanghai, China) for 1 h. The cells were washed in PBS buffer for 25 min, followed by incubation with 6′-diamidino-2-phenylindole (DAPI) for 10 min (Beyotime Biotechnology, Shanghai, China). These immunostained cells were visualized by indirect fluorescence under the fluorescent microscope (DMI 4000B, Leica, Germany). Furthermore, immunofluorescent staining for Heme Oxygenase (HO)-1 in rat brain sections was also performed in the animal experiment. The protocol was similar with that described above. The HO-1 rabbit polyclonal antibody (Santa Cruz, Dallas, TX, USA) was diluted to 1: 200.

2.6 Animal experiments

2.6.1 ICH surgery

The animal protocols were approved by the Animal Ethics Committee of Third Military Medical University, China. Male Sprague–Dawley rats (300–350 g) were housed under standard 12:12 h light–dark conditions and allowed free access to food and water. The model of ICH in rats were conducted by intrastriatal injection of autologous whole blood as previously described (Wu et al., 2003). Briefly, the rats were anesthetized intraperitoneally (i.p.) with chloral hydrate at a concentration of 100 mg/kg and placed in a stereotaxic frame. The rats received an autologous whole blood (50 μL) injection into the right basal ganglia (coordinates: 0.2 mm anterior, 3.5 mm lateral, and 5.5 mm ventral to the bregma) through a 26-gauge needle.

After 4 h, the aspiration surgery was carried out using a previously described method (Altumbabic et al., 1998). The rats were anesthetized with chloral hydrate (100 mg/kg, i.p.) and placed in the stereotactic frame. Streptokinase (10 μL; 300 U/μL, Sigma) was injected into the core of hematoma by a 26-gauge needle. 1 hour later, the lysed blood was aspirated with a syringe attached to a 26-gauge needle placed at the same stereotactic coordinates, and the skull hole was closed with bone wax.

2.6.2 Experimental groups

ICH rats after aspiration surgery were randomly divided into MH-treated (ICH+Surgery+MH), MH-loaded KG-treated (ICH+Surgery+KG) and vehicle-treated groups (ICH+Surgery+Vehicle). MH was administrated intraperitoneally (i.p.) after the aspiration surgery with 45 mg/kg. MH-loaded KG (20 μL) was injected by a 26-gauge needle into the core of hematoma after the aspiration surgery. The concentration of keratose was 20 %, and the MH concentrations in KG were 0.1, 1.0, and 10.0 mg/mL, respectively. While, vehicle-treated group was injected 20 μL sterile saline under the same conditions. Furthermore, the empty needle was inserted twice into the right basal ganglia of ICH rats in the ICH+sham group.

2.6.3 Histology

The rats were anesthetized and underwent intracardiac perfusion with 4 % paraformaldehyde in 0.1 mol/L PBS buffer (pH 7.4). The brains were removed and kept in 4 % paraformaldehyde for 24 h, and immersed in 30 % sucrose for 3 d at 4 °C. Then the brains were cut into 30-mm-thick coronal sections with a cryostat (Leica CM1900, Germany).

Iron deposition was evaluated with enhanced Perls' staining. Brain sections were incubated in Perls' solutions (1:1, 5 % potassium ferrocyanide and 5 % HCl) for 45 min, washed using distilled water, and then incubated in 0.5 % diamine benzidine tetrahydrochloride with nickel for 60 min. In addition, the rats were euthanized at days 3 after ICH followed by different treatments. The organs including the heart, lung, spleen, kidney, and liver were performed with hematoxylin and eosin (H&E) stains and observed.

2.6.4 Brain water and iron contents

Brain edema was determined by the wet–dry weight ratio method as described previously (Okauchi et al., 2009). After blood infusion for 24 h, rats were euthanized. The brain tissue slice was divided into 2 hemispheres along the midline. The white matter tissue adjacent to the hematoma, including superficial gyral white matter and

deep white matter, was collected. The brain tissue was placed on foils and weighed by an electronic analytic balance (ME204E, Mettler Toledo, China) to obtain the wet weight. Samples were then dried in a gravity oven at 100 °C for 24 h to obtain the dry weight. Brain water content (%) was calculated as ([wet weight − dry weight]/ wet weight) × 100 %.

Total brain iron concentration (μg/g of tissue; wet weight) was measured by graphite furnace atomic absorption spectrophotometer (Z-2700, Hitachi, Japan) according to the standard protocol. A coronal slice 4 mm thick around the injection needle tract was cut, divided into ipsilateral and contralateral sides, and weighed. 100 mg tissue around hematoma was wet-digested with 1 mL of 1 mol/L nitric acid for 1 week.

2.6.5 Neurobehavioral tests

Neurological deficits were assessed using the corner turn and forelimb-placing tests. For the corner turn test, the rat was allowed to proceed into a corner with the angle of 30°. To exit the corner, the animal could turn either left or right, and the direction was recorded. This tests were repeated 10 times and the percentage of right turns was calculated. In the vibrissae-elicited forelimb-placing test, rats were held by their bodies to allow the forelimbs to hang free. Independent testing of each forelimb was conducted by brushing the respective vibrissae on the corner of a tabletop once per trial for 10 trials. The percentage of successful placing responses was determined for the impaired and the unimpaired forelimbs.

2.6.6 Western blotting

Rats were anesthetized and killed at days 3 after ICH for western blot analysis. Briefly, brain tissue was immersed in the Western sample buffer and sonicated. Protein concentration was determined by Bio-Rad protein assay kit. The protein (30 μg) from each sample was separated by 10% SDS-PAGE and transferred to PVDF membranes. The primary antibody was polyclonal rabbit anti-rat HO-1, (Santa Cruz, Dallas, TX, USA) and the secondary antibody was goat anti-rabbit IgG (Zhongshan, Beijing, China).

Blot for β-actin (4A Biotech, China) was served as a control to ensure constant protein loading level. The antigen-antibody complexes were visualized by chemiluminescence (ECL detection system; PerkinElmer Life Sciences). The intensities of bands were quantified by image analyzing software (Quantity One, Bio-rad).

2.7 Biocompatibility of KGs

Rats were anesthetized with chloral hydrate (100 mg/kg, i.p.) and placed in a stereotaxic frame. 50 μL blank KG (20 %) was injected into the right basal ganglia as the procedure of ICH surgery. The rats were euthanized and organs including the heart, lung, spleen, kidney, and liver were performed with hematoxylin and eosin (H&E) stains at appropriate time points (7, 14, 21, and 28 d) and observed. In addition, the histological examination of rat brain after injection of KG was also performed.

2.8 Statistics

All measurements were performed at least in triplicate and data were presented as mean ± standard deviation (S.D.). For the selected evaluation tests, single comparisons were analyzed by Students t-test or paired Student's t-test. For multiple comparisons, one-way ANOVA was applied followed by Tukey post hoc analysis. The statistical significance level (P) was set at $P < 0.05$ and statistically highly significant as $P < 0.01$.

3. RESULTS

3.1 Keratose extraction and characterizations

The molecular weight of keratose was analyzed through SDS-PAGE (Fig. S1). The distinct band of 40–60 kDa represented the main molecular weight of keratose, which was consistent with the previous report (Wang et al., 2017). Furthermore, the amino acid composition of keratose was evaluated. 16 amino acids included 63.37 % ± 4.07 (n = 3) of hydrophilic amino acid were identified within the keratose (Fig. S2). Glutamic Acid was the largest proportion of amino acid in the keratose extracts, while the lowest one was histidine.

3.2 KG preparation and characterizations

3.2.1 Morphology

The morphology of KG with 20 % keratose prepared by lyophilization was observed by SEM. As illustrated in Fig. 1, the KG exhibited a porous structure, which would contribute to iron adsorption.

3.2.2 FT-IR Analysis

FT-IR analysis was carried out to characterize the potential chemical changes within the formation of MH-loaded KG. The infrared spectra of MH, keratose and MH-loaded KG (20 % keratose and 1.0 mg/mL MH) are illustrated in Fig. 2A. The characteristic peaks of MH were found at 1610 cm^{-1} (C=O stretching vibration at rings A), 1580 cm^{-1} (C=O stretching vibration at rings C), 1244 cm^{-1} (C–N amine stretching vibration), 1176 cm^{-1} (phenolic C–O stretching band), and 870 cm^{-1} (C-O stretching vibration) (Brigante and Schulz, 2012). Keratose showed the characteristic peaks at 2800– 4000 cm^{-1} associated to amide A bands, 1600– 1700 cm^{-1} associated to amide I bands, 1480–1580 cm^{-1} associated to amide II bands, 1220–1330 cm^{-1} associated to amide III bands (Wang et al., 2017). These major functional groups were also observed in the MH-loaded KG spectra. Therefore, no new bond was found in the spectrum of MH-loaded KG, which indicated that no chemical interaction between keratose and MH during the hydrogel preparation.

3.2.3 XRD analysis

The XRD patterns of MH, keratose and MH-loaded KG (20 % keratose and 1.0 mg/mL MH) are shown in Fig. 2B. Several distinctive peaks were found ranging from 5° to 45° in the diffractogram of MH, and there was a prominent 2θ peak at 22.5° in the diffractogram of keratose, displaying an amorphous structure. Moreover, the peaks of MH and keratose were observed for MH-loaded KG, indicating no change between MH and keratose in the formulation of KG.

3.2.4 Adsorption experiments

Fig. 2C shows the effect of contact time on the adsorption capacity of KG with different concentrations of keratose (ranging from 10 % to 40 %) for Fe^{2+} ions. The adsorption rate was fast initially, and approximately 90 % of total Fe^{2+} ions was removed within 30 min. Then a relatively slow adsorption rate was observed until equilibrium was reached at 60 min. Additionally, the adsorption capacity of adsorbent slightly increased with increasing KG concentrations, and KG with the concentration of 40 % could reach the saturation states within 30 min.

3.2.5 In vitro drug release

The *in vitro* release profiles of MH from MH-loaded-KG (20 % keratose and 1.0 mg/mL MH) in the artificial CSF (pH 7.4) are shown in Fig. 2D. MH displayed an initial fast release within 120 min, which was attributed to the porous structure of KG. However, the sustained-release phase was observed in the release profile after 120 min, approximately 80 % of MH released from KG over a period of 720 min.

3.3 In vitro cytotoxicity and cytoprotective studies

3.3.1 In vitro cytotoxicity studies

The *in vitro* cytotoxicities of blank KG and MH-loaded KG (20 % keratose and 1.0 mg/mL MH) were evaluated by the MTT assay using primary neuronal cells. The percentage of cell growth inhibition was assayed as the cells survived after the specific periods of incubation. Fig. 3A shows the cytotoxicity of different concentrations of blank KG (20 % keratose) after incubation for 24 h. Cell viability significantly decreased when exposed to increasing concentrations above 100 mg/L of blank KG ($P < 0.05$). Moreover, there was a highly significant decline of cell viability after incubation with MH-loaded KG at a concentration of 200 mg/L for 24 h ($P < 0.01$) (Fig. 3B), but an increase in cytotoxicity was observed as the concentration of drug-loaded KG increased. The results indicated that KG displayed a slight *in vitro* cytotoxicity, whereas the relatively high cytotoxicity of drug-loaded KG was resulted from the toxicity of MH itself.

3.3.2 In vitro cytoprotective studies

The *in vitro* neuronal cell injury model was established as previously described (Regan and Rogers, 2003). Different concentrations of hemoglobin (ranging from 6.25 to 100 μM) were added into cell-culture media. A gradual decrease in cell viability with increasing hemoglobin concentration was shown (Fig. S3). A highly significant decline of cell viability was observed at the hemoglobin concentration of 6.25 μM ($P < 0.01$). Furthermore, the *in vitro* cytoprotective effects of blank KG (20 % keratose) and MH-loaded KG (20 % keratose and 1.0 mg/mL MH) were also investigated by the addition of KGs (50 μM) to hemoglobin-treated cells. Fig. 3C shows the cytoprotective effect of blank KG against hemoglobin toxicity at different concentrations (ranging from 0 to 400 mg/L). Blank KG played a role in the reduction of hemoglobin toxicity. The increase of KG concentration led to enhance cell viability, which probably resulted from the adsorption performance of KG for iron. However, MH-loaded KG displayed a stronger cytoprotective effect than blank KG (Fig. 3D). This could be attributed to the combined effects of iron adsorption of hydrogels and iron chelation of MH. Thus, a highly significant increase in the cell viability was found when the concentration of MH-loaded KG increased to 50 mg/L ($P < 0.01$). The cell viability reachedapproximately 90 % and 70 % for 400 mg/L of MH-loaded KG and KG after treating injured cells, respectively.

Moreover, the image of primary neuronal cell culture showed neuronal staining with MAP-2 (green), and cells were counterstained with DAPI solution to identify the nuclei of cells (blue). Fig. 4 shows the effects of different treatments on immunofluorescence staining of primary neuronal cells incubated with hemoglobin, and the fluorescence intensity of MAP-2 was shown in Fig. 5. Compared to the control group (Fig. 4A), the number of MAP2/DAPI-positive cells was significantly increased by the addition of KG ($P < 0.05$) and MH-loaded KG ($P < 0.01$). Furthermore, more MAP-2/DAPI positive neurons were observed with MH-loaded KG than that of blank KG ($P < 0.01$) (Figs. 4B and C), suggesting that MH-loaded KG had a stronger cytoprotective effect than blank KG.

3.4 ICH postoperative treatment by KG

3.4.1 Iron deposition

Iron release from the breakdown of hemoglobin was observed by enhanced Perl's reaction. Fig. 6 shows iron histochemistry in the contralateral and ipsilateral basal ganglia on day 3 after ICH, and iron staining was exhibited in Fig. 7. Postoperative treatments by MH and MH-loaded KG could significantly reduce iron deposition on day 3 after ICH, and less iron deposition was observed in the ICH+surgery+KG group compared with ICH+surgery+MH and ICH+surgery+vehicle groups ($P < 0.01$). Furthermore, the increase of MH concentration within the KG led to a significant decrease in iron deposition.

3.4.2 Brain iron content

Iron contents of total brain tissue were detected using graphite furnace atomic absorption spectrophotometer (Fig. 8A). An increase of brain iron level in the ipsilateral hemisphere after ICH was found (109.50 μg/g vs. 52.48 μg/g in the contralateral side). Hematoma aspiration initiated at 4 h after ICH could reduce the brain iron (92.23 μg/g vs. 109.50 μg/g in the ICH+sham group, $P < 0.01$), but the treatment with 0.1 mg/mL of MH by MH (i.p.) and MH-loaded KGdid not significantly decrease the ICH-induced iron deposition. Differently, a significant reduction in brain iron content was observed after postoperative MH-loaded KG treatments with 1.0 and 10 mg/mL of MH (74.69 μg/g and 72.13 μg/g of ipsilateral respectively; $P < 0.05$ vs. ICH+surgery+vehicle group). Furthermore, less brain iron content was detected after postoperative KG treatments with 1.0 and 10 mg/mL of MH respectively compared to the postoperative MH treatment ($P<0.05$ vs. ICH+surgery+MH group).

3.4.3 Brain edema

The effect of postoperative MH-loaded KG treatments on brain edema formation in rats was assessed on day 3 after induction of ICH followed by aspiration surgery (Fig. 8B). Brain water content in ICH rats was highly significantly attenuated by hematoma

aspiration ($P < 0.01$, vs. ICH+sham group), and systemic administration of MH (45 mg/kg, i.p.) after aspiration surgery could significantly reduce the brain edema ($P < 0.05$, vs. ICH+surgery+vehicle group). In addition, MH-loaded KG with different dose strengths of MH (0.1, 1.0, and 10 mg/mL) also significantly reduced ICH-induced brain edema ($P < 0.05$, vs. ICH+surgery+vehicle group), which displayed a stronger therapeutic effect on brain edema comparted to the postoperative MH treatment ($P < 0.05$, vs. ICH+surgery+MH group). The amelioration of ICH induced edema formation with MH-loaded KG was associated with a reduced iron accumulation in the ipsilateral basal ganglia.

3.4.4 Neurological deficits

To examine the effect of MH-loaded KG on neurobehavioral deficits after ICH aspiration surgery, the behavioral tests, including the forelimb-placing and corner turn tests, were performed before ICH and 1, 3, 7, 14, 21, and 28 d after ICH aspiration surgery. Postoperative MH-loaded KG treatment improved the recovery of ICH-induced forelimb-placing deficit in rats (Fig. 8C). A significant recovery of forelimb-placing at 3, 7, 14, 21, and 28 d after the ICH aspiration surgery ($P < 0.05$, vs. ICH+sham group), but postoperative MH treatment did not significantly improve the forelimb-placing deficit compared to the ICH+surgery+vehicle group. Moreover, postoperative MH-loaded KG significantly ameliorated ICH-induced forelimb-placing deficit occurred with time ($P < 0.01$, vs. ICH+surgery+vehicle group), which also showed a significantly better postoperative recovery than that in MH-treated group ($P < 0.01$).

For the corner turn test, aspiration surgery showed significant neurological improvement at all time points compared to the ICH group ($P < 0.05$ and $P < 0.01$, Fig. 8D). Both the postoperative MH (i.p.) and MH-loaded KG treatments exhibited significant improvement in corner-turn deficit ($P < 0.05$ and $P < 0.01$ vs. ICH+surgery+vehicle group). Furthermore, ICH-rats treated with MH-loaded KG after aspiration surgery showed a highly significant improvement in corner-turn deficit compared to postoperative MH treatment ($P < 0.01$). Overall, the significant recovery

of neurological function was observed in all postoperative MH-loaded KG treatment groups, but the neurological functions were not significantly improved with increasing MH concentration.

3.4.5 HO-1 expression

HO-1, a key heme degradation enzyme, is expressed very low in the normal brain of the adult rat. Western blot analysis showed a decrease in level of HO-1 protein in the basal ganglia after 3 d of aspiration surgery (Fig. 9A). HO-1 was decreased by the postoperative MH treatment ($P <$ 0.05, versus ICH+surgery+vehicle group), and a highly significant reduction in HO-1 protein was found with the postoperative treatment of MH-loaded KG ($P < 0.01$, versus ICH+surgery+vehicle group). The level of HO-1 protein was also decreased markedly with increasing MH concentration within the KG.

HO-1 immunofluorescence was strong in the perihematomal zone of ICH rats (Fig. 9B), while it decreased around the haematoma site at 1 d after aspiration surgery. HO-1 positive cells were detected with a postoperative intraperitoneal injection of MH, whereas less HO-1 positive cells were found in the ICH+surgery+KG groups. The increase of MH concentration led to the decrease in HO-1 positive cells.

3.5 In vivo biocompatibility

To observe the biodegradation of KG in the brain, the pure KG was injected into the right basal ganglia following the ICH surgery procedure (Fig. 10). The volume of KG decreased over time, and few amounts of KG were found at 28 d after intracerebral infusion.

Furthermore, H&E staining of major organs was carried out to investigate the systemic toxicity of implants (Fig. S4), no significant histopathological differences of the organs were observed among the different groups. More specifically, no pathological features were found in the organs, which included partial myocardial cells disordered infiltration, congestion of scattered inflammatory cells in the liver tissue, and appearance of renal interstitial hyperemia. The results suggested that the intracerebral infusion of KG would not produce systemic toxicity *in vivo*.

4. DISCUSSION

Surgical treatment for ICH is a common and necessary strategy in the clinic, especially for patients with a large lobar ICH. However, the role of surgery for most patients with ICH remains controversial, because no clear benefit from the surgical treatment was identified from the randomized trials by comparing surgery with conservative management (Hemphill et al., 2015). Moreover, secondary injury caused by blood breakdown and adverse biochemical or inflammatory processes would continue after ICH surgery due to the low clot clearance rate. Therefore, we hypothesized that the postoperative functional recovery would be improved by in situ injection of MH-loaded KG into the hematoma region. The direct brain injection of hydrogel is unacceptable for the ICH patients with conservative management, but the ICH aspiration surgery provides an opportunity for hydrogel implantation. Some biomaterials have been widely used as standard tools in neurosurgery in the recent years.

Keratose, an oxidized form of keratin, was used for hydrogel formation and locally injected into the hematoma region to improve the postoperative functional recovery of ICH rats in this study. Keratins from human hairs have been used for nerve regeneration, wound healing, hemostasis, bone regeneration and cell culture because of its excellent biocompatibility, degradability, non-immunogenic nature, cellular attachment, proliferation and viability features (Wang et al., 2016). The *in vivo* biocompatibility was evaluated by implanting keratose in the subcutaneous layer, and the relative area of keratose implants decreased to 92 % at the 8-week time point (de Guzman et al., 2011). However, keratose displayed a fast biodegradation in the brain, and most KG degraded at days 28 after intracerebral infusion in this study. Additionally, ordered internal cell architecture made up of isolated and interconnected pores could be easily formed via the lyophilization of keratose, and the porous structure of hydrogel would be beneficial to the iron adsorption.

Fast adsorption of iron in the hematoma region is favorable for the reduction of iron overload. Free iron levels in the normal CSF were 1.1 ± 0.4 μmol in rats, while ones in CSF increased to 14.25 ± 5.0 μmol at days 3 after ICH. Therefore, 20 μmol was

selected as the initial concentration of Fe^{2+} in the adsorption experiments. KG displayed a good adsorptive property due to its porous structure, and the concentration of Fe^{2+} in the artificial CSF decreased to 1.64 μmol after incubation with KG (20 % keratose) for 30 min (Fig. S5). The results suggested that the iron overload would be attenuated temporarily by the adsorptive property of blank KG. The cytoprotection was also observed by the addition of blank KG to hemoglobin-treated cells. However, the iron still retain in the blank KG, and the cytotoxicity of iron would appear again when the hydrogel began degradation. Therefore, the blank KG is not suitable for the treatment of iron overload after ICH, because it can attenuate the iron overload temporarily rather than eliminate the iron thoroughly. The blank KG group was not selected to compare the effects of blank KG with MH-loaded KG in the subsequent *in vivo* studies.

MH has been investigated about its potential to reduce iron overload and neuronal death following ICH. Few human pilot studies have been conducted to investigate the efficacy of MH treatment following hemorrhage or traumatic brain injury (Garton et al., 2016). MH was intraperitoneally administrated at 45 mg/kg to decrease iron overload and brain injury after ICH in rats (Zhao et al., 2011), while local delivery strategy could reduce dose strength of MH due to the absence of blood-brain barrier. 20 μL of MH-loaded KGs with different MH concentrations (0.1, 1.0 and 10.0 mg/mL) was injected into the hematoma region to attenuate iron-induced brain injury in the present study. The increase of MH concentration in KG led to decrease iron deposition, brain iron content, brain edema, and enhance neurological functional recovery. However, the survival rate of rats decreased after treated with KG high MH concentration (10.0 mg/mL).

The 28-day survival rate of ICH rats was 100 % (15/15), whereas it decreased to 93.33 % (14/15) after aspiration surgery (Fig. 11). In addition, increasing MH concentration led to reduce the survival rate of rats. The 28-day survival rate of rats in ICH+surgery+KG group with 0.1 mg/mL, 1.0 mg/mL, and 10.0 mg/mL of MH was 93.33 % (14/15), 86.67 % (13/15), and 53.33 % (8/15), respectively. Compared to KG, ICH rats treated with MH solution (i.p.) showed survival rate of 80.00 % (12/15). Furthermore, most of the rats died at day 1 and days 3 after ICH aspiration surgery.

5. CONCLUSIONS

Iron chelators have great potential to improve the functional recovery after ICH by reducing iron overload. In this study, we focused on the postoperative functional recovery after ICH. The MH-loaded KG was prepared and locally injected into the hematoma region after ICH aspiration surgery in rats. Hydrogel could quickly adsorb the non-heme iron and keep sustained release of iron chelator in the hematoma region, so it supplied a high iron-chelating efficiency and decreased the systemic adverse events by reducing dose strength. Compared to the systemic administration of MH (approximately 15 mg, i.p.), in situ injection of KG loading with 1.0 mg/mL of MH (20 μg) showed a better postoperative functional recovery of ICH in rats. Furthermore, the survival rate of ICH rats treated with aspiration surgery followed by KG injection (0.1 and 1.0 mg/mL of MH) was higher than that by postoperative MH administration. However, we also found that high dose strength of MH in KG (10.0 mg/mL) influenced the survival rate of ICH rats. These results suggested in situ injection of hydrogel loaded with iron chelator after aspiration surgery could be a new therapeutic strategy for the enhancement of postoperative functional recovery after ICH.

ACHNOWLEDGEMENTS

The authors acknowledge the financial assistance provided by the National Basic Research Program of China (Grant No. 2014CB541603), the National Natural Science Foundation of China (Grant No. 31600770), and the Fundamental Research Funds for the Central Universities (Grant No. 10611CDJXZ238826). Furthermore, we thank B.S. Med Li C.H. who suffered from ICH and encouraged us to study on the basic and translational stroke research. Finally, we thank Prof. Jing Peng, and Prof. Nina Mo (School of Foreign Language and Cultures, Chongqing University) for their efforts in English editing.

References

Altumbabic, M., Peeling, J., Del Bigio, M.R., 1998. Intracerebral hemorrhage in the rat: effects of hematoma aspiration. Stroke 29, 1917-1923.

Andrew, R., MacVicar, B., 1994. Imaging cell volume changes and neuronal excitation in the hippocampal slice. Neuroscience 62, 371-383.

Balami, J.S., Buchan, A.M., 2012. Complications of intracerebral haemorrhage. Lancet Neurol 11, 101-118.

Borges, V.M., Lee, T.W., Christie, D.L., Birch, N.P., 2010. Neuroserpin regulates the density of dendritic protrusions and dendritic spine shape in cultured hippocampal neurons. J Neurosci Res 88, 2610-2617.

Brigante, M., Schulz, P.C., 2012. Adsorption of the antibiotic minocycline on cerium (IV) oxide: Effect of pH, ionic strength and temperature. Micropor Mesopor Mater 156, 138-144.

de Guzman, R.C., Merrill, M.R., Richter, J.R., Hamzi, R.I., Greengauz-Roberts, O.K., Van Dyke, M.E., 2011. Mechanical and biological properties of keratose biomaterials. Biomaterials 32, 8205-8217.

de Guzman, R.C., Saul, J.M., Ellenburg, M.D., Merrill, M.R., Coan, H.B., Smith, T.L., Van Dyke, M.E., 2013. Bone regeneration with BMP-2 delivered from keratose scaffolds. Biomaterials 34, 1644-1656.

Flaherty, M.L., Beck, J., 2013. Surgery for Intracerebral Hemorrhage. Stroke 44, 2953-2954.

Gao, H., Sun, Y., Zhou, J., Xu, R., Duan, H., 2013. Mussel-inspired synthesis of polydopamine-functionalized graphene hydrogel as reusable adsorbents for water purification. Acs Appl Mater Interfaces 5, 425-432.

Garton, T., Keep, R.F., Hua, Y., Xi, G., 2016. Brain iron overload following intracranial haemorrhage. Stroke and Vascular Neurology, e000042.

Hemphill, J.C., Greenberg, S.M., Anderson, C.S., Becker, K., Bendok, B.R., Cushman, M., Fung, G.L., Goldstein, J.N., Macdonald, R.L., Mitchell, P.H., 2015. Guidelines for the management of spontaneous intracerebral hemorrhage. Stroke 46, 2032-2060.

Hill, P., Brantley, H., Van Dyke, M., 2010. Some properties of keratin biomaterials: kerateines. Biomaterials 31, 585-593.

Kumar, S., Selim, M., Marchina, S., Caplan, L.R., 2016. Transient Neurological Symptoms in Patients With Intracerebral Hemorrhage. JAMA neurology 73, 316-320.

Lee, T.W., Tumanov, S., Villas‐Bôas, S.G., Montgomery, J.M., Birch, N.P., 2015. Chemicals eluting from disposable plastic syringes and syringe filters alter neurite growth, axogenesis and the microtubule cytoskeleton in cultured hippocampal neurons. J Neurochem 133, 53-65.

Mayer, S.A., 2003. Ultra-early hemostatic therapy for intracerebral hemorrhage. Stroke 34, 224-229.

Mayer, S.A., Rincon, F., 2005. Treatment of intracerebral haemorrhage. Lancet Neurol 4, 662–672.

Mendelow, A.D., Gregson, B.A., Fernandes, H.M., Murray, G.D., Teasdale, G.M., Hope, D.T., Karimi, A., Shaw, M.D.M., Barer, D.H., investigators, S., 2005. Early surgery versus initial conservative treatment in patients with spontaneous supratentorial intracerebral haematomas in the International Surgical Trial in Intracerebral Haemorrhage (STICH): a randomised trial. The Lancet 365, 387-397.

Mendelow, A.D., Gregson, B.A., Rowan, E.N., Murray, G.D., Gholkar, A., Mitchell, P.M., Investigators, S.I., 2013. Early surgery versus initial conservative treatment in patients with spontaneous supratentorial lobar intracerebral haematomas (STICH II): a randomised trial. The Lancet 382, 397-408.

Morgan, T., Zuccarello, M., Narayan, R., Keyl, P., Lane, K., Hanley, D., 2008. Preliminary findings of the minimally-invasive surgery plus rtPA for intracerebral hemorrhage evacuation (MISTIE) clinical trial, Cerebral Hemorrhage. Springer, pp. 147-151.

Ochalski, P., Chivukula, S., Shin, S., Prevedello, D., Engh, J., 2014. Outcomes after endoscopic port surgery for spontaneous intracerebral hematomas. Journal of Neurological Surgery Part A: Central European Neurosurgery 75, 195-206.

Okauchi, M., Hua, Y., Keep, R.F., Morgenstern, L.B., Xi, G., 2009. Effects of deferoxamine on intracerebral hemorrhage-induced brain injury in aged rats. Stroke 40, 1858-1863.

Pace, L.A., Plate, J.F., Smith, T.L., Van Dyke, M.E., 2013. The effect of human hair keratin hydrogel on early cellular response to sciatic nerve injury in a rat model. Biomaterials 34, 5907-5914.

Qureshi, A.I., Mendelow, A.D., Hanley, D.F., 2009. Intracerebral haemorrhage. The Lancet 373, 1632-1644.

Rabinstein, A.A., 2017. Intracerebral haemorrhage: no good treatment but treatment helps. The Lancet.

Regan, R.F., Rogers, B., 2003. Delayed treatment of hemoglobin neurotoxicity. J Neurotraum 20, 111-120.

Selim, M., Yeatts, S., Goldstein, J.N., Gomes, J., Greenberg, S., Morgenstern, L.B., Schlaug, G., Torbey, M., Waldman, B., Xi, G., 2011. Safety and tolerability of deferoxamine mesylate in patients with acute intracerebral hemorrhage. Stroke 42, 3067-3074.

Sierpinski, P., Garrett, J., Ma, J., Apel, P., Klorig, D., Smith, T., Koman, L.A., Atala, A., Van Dyke, M., 2008. The use of keratin biomaterials derived from human hair for the promotion of rapid regeneration of peripheral nerves. Biomaterials 29, 118-128.

Wang, J., Hao, S., Luo, T., Yang, Q., Wang, B., 2016. Development of feather keratin nanoparticles and investigation of their hemostatic efficacy. Mat Sci Eng C-Mater 68, 768-773.

Wang, J., Hao, S., Luo, T., Zhou, T., Yang, X., Wang, B., 2017. Keratose/poly (vinyl alcohol) blended nanofibers: Fabrication and biocompatibility assessment. Mat Sci Eng C-Mater 72, 212-219.

Wang, S.-L., Chen, C.-C., Tzou, Y.-M., Hsu, C.-L., Chen, J.-H., Lin, C.-F., 2009. A mechanism study of light-induced Cr (VI) reduction in an acidic solution. J Hazard Mater 164, 223-228.

Wu, H., Wu, T., Xu, X., Wang, J., Wang, J., 2011. Iron toxicity in mice with collagenase-induced intracerebral hemorrhage. Journal of Cerebral Blood Flow & Metabolism 31, 1243-1250.

Wu, J., Hua, Y., Keep, R.F., Nakamura, T., Hoff, J.T., Xi, G., 2003. Iron and iron-handling proteins in the brain after intracerebral hemorrhage. Stroke 34, 2964-2969.

Xi, G., Keep, R.F., Hoff, J.T., 2006. Mechanisms of brain injury after intracerebral haemorrhage. Lancet Neurol 5, 53-63.

Xi, G., Strahle, J., Hua, Y., Keep, R.F., 2014. Progress in translational research on intracerebral hemorrhage: is there an end in sight? Prog Neurobiol 115, 45-63.

Xiong, X.-Y., Wang, J., Qian, Z.-M., Yang, Q.-W., 2014. Iron and intracerebral hemorrhage: from mechanism to translation. Transl Stroke Res 5, 429-441.

Yeatts, S.D., Palesch, Y.Y., Moy, C.S., Selim, M., 2013. High dose deferoxamine in intracerebral hemorrhage (HI-DEF) trial: rationale, design, and methods. Neurocritical care 19, 257-266.

Zhao, F., Hua, Y., He, Y., Keep, R.F., Xi, G., 2011. Minocycline-induced attenuation of iron overload and brain injury after experimental intracerebral hemorrhage. Stroke 42, 3587-3593.

Figure Captions

Fig. 1. SEM images of KG at different magnifications.

Fig. 2. The FTIR spectra (A) and XRD diffraction patterns (B) of keratose, MH and MH-loaded KG. Adsorption behaviors (C) of iron (II) on KG with different keratose concentrations. *In vitro* release profiles (D) of MH from the KG with 20 % of keratose.

Fig. 3. Cytotoxicity of blank KG (A) and MH-loaded KG (B) with different concentrations toward primary neuronal cells. Protective effect of delayed treatment with blank KG (C) and MH-loaded KG (D) with different concentrations. Cells were treated with 50 mM hemoglobin alone, and blank KG or MH-loaded KG added 4 h after hemoglobin. (n=6, *P < 0.05, **P < 0.01).

Fig. 4. Immunofluorescence staining of primary neuronal cells incubated with hemoglobin in the absence (A) and presence of blank KG (B) or MH-loaded KG (C). Immunostaining for the dendritic marker protein MAP-2 (green), and DAPI staining (blue) denotes cell nuclei (original magnification, ×100).

Fig. 5. Fluorescence intensities of MAP-2 in neuronal samples after treated with hemoglobin, blank KG and MH-loaded KG in vitro. (n = 6, *P < 0.05, **P < 0.01).

Fig. 6. Iron histochemistry (Perls' staining) in contralateral and ipsilateral basal ganglia at days 3 after ICH.

Fig. 7 Iron staining in contralateral and ipsilateral basal ganglia at days 3 after ICH. (n = 6, *P < 0.05, **P < 0.01).

Fig. 8. Brain iron content (A) and brain water content (B) in white matter at days 3 after ICH. Forelimb-placing (C) and corner turn (D) test before ICH and 1, 3, 7, 14, 21, and 28 d after ICH. (n=6, *P < 0.05, **P < 0.01).

Fig. 9. Western blot analysis showing HO-1 (A) and HO-1 immunoexpression (B) in the ipsilateral basal ganglia at days 3 after ICH. Bar graph quantifies the Western blotting. (n=6, *P < 0.05, **P < 0.01).

Fig. 10. Histological analysis of KG in the brain at different time points after intracerebral infusion (A-D), and magnified images with a magnification of × 100 (E-H).

Fig. 11. The survival rate of rats in different treatment groups. The survival curves of rats (n=15) with indicated treatment were monitored.